Desalination and Water Treatment
www.deswater.com
doi: 10.5004/dwt.2023.29808

304 (2023) 169–180
August

Response surface methodology for adsorption of propylparaben using zeolitic imidazolate-67 modified by Fe_3O_4 nanoparticles from aqueous solutions

Mohammad Pourmohammad[a], Arezoo Ghadi[a,*], Ali Aghababai Beni[b]

[a]*Department of Chemical Engineering, Ayatollah Amoli Branch, Islamic Azad University, Amol, Iran, emails: arezoo.ghadi@gmail.com (A. Ghadi), mohammad.pourmohammad@yahoo.com (M. Pourmohammad)*
[b]*Department of Chemical Engineering, Shahrekord Branch, Islamic Azad University, Shahrekord, Iran, email: aliaghababai@yahoo.com*

Received 27 March 2023; Accepted 1 July 2023

ABSTRACT

The applicability of zeolitic imidazolate-67 modified by Fe_3O_4 nanoparticles, was studied for removing of propylparaben from aqueous solutions by adsorption method using response surface methodology. For the adsorption characterization of the adsorbent used in propylparaben adsorption, Brunauer–Emmett–Teller, Fourier-transform infrared spectroscopy, and scanning electron microscopy analyses were performed and the findings were compared. The impacts of variables, including initial propylparaben concentration (X_1), pH (X_2), adsorbent dosage (X_3), and sonication time (X_4), the highest removal efficiency was obtained as 98%, 10 mg·L^{-1} initial concentration, pH 6, 0.025 g adsorbent concentration, and 5 min contact time, respectively. The experimental data obtained were applied to the adsorption equilibrium and kinetic data it was seen that the data were for the Langmuir isotherm, pseudo-second-order kinetics, and maximum adsorption capacity (117.5 mg·g^{-1}), respectively. Promising treatment capabilities of the ZIF-67-Fe_3O_4NPs have been during the comparative adsorption removal of propylparaben from deionized water against spiked natural water samples and synthetic Na^+, K^+, Ca^{2+}, and Mg^{2+} solutions. Overall results confirmed that ZIF-67-Fe_3O_4NPs like being recyclable, and cost-efficient made it a promising material for aqueous solutions.

Keywords: Propylparaben; Adsorption capacity; Zeolitic imidazolate-67; Central composite design (CCD); Response surface methodology (RSM)

1. Introduction

Parabens, as an undesirable by-product, may to a sanitary sewer or surface water in the environment. Therefore, this issue has been among the most severe environmental concerns to keep an eye on [1]. Parabens are chemical esters of p-hydroxybenzoic acid and are a class of widely used artificial preservatives and antimicrobials in many PCPs (personal care products), and pharmaceutical products [1,2]. The use of parabens in sunscreen creams, toothpaste, cosmetics, glues, fats, and oils is inevitable, and their use in various consumer products is undeniable [2–4]. Also, some scholars, in their published studies, have associated the high concentrations of parabens with male reproductive disorders. However, paraben has found its way to wastewater plants due to its large-mentioned application. For removing parabens from aqueous media, different methods of cloud point extraction, membrane filtration, electrochemical techniques, adsorption, and biosorption have been practised [5–9]. Particularly, adsorption has drawn the attention of worldwide researchers, thanks to simplicity in operation, high efficiency, and inexpensive operation cost [10,11]. In improving removal efficiency, detecting novel adsorbent materials has always been the most prominent issue in adsorption [12].

* Corresponding author.

Conventional adsorbents have presented a significant challenge in terms of selectivity and capacity. In recent years, metal–organic frameworks (MOFs) have emerged as promising alternative in various applications, including adsorption processes [13–15]. Among the MOFs, a specific class known as zeolitic imidazolate frameworks (ZIFs) has garnered attention. These frameworks are formed by imidazole linkers and zinc or cobalt ions, resulting in microporous crystalline structures that exhibit characteristics of both MOFs and zeolites [16,17]. ZIFs possess distinct porous structures with open frameworks, adjustable cage pore structures, large surface areas, exceptional functionalities, and improved thermal and chemical stabilities. These unique properties make them suitable for a wide range of potential applications, including adsorption, catalysis, separation, and sensing [18,19].

Nowadays, the dyes in the fashion industry in the sewage system can have a negative impact on the environment. However, wastewater from the fashion industry getting will be more to handle. Among modern treatment technologies, adsorption is an effective treatment [20,21]. Zeolitic imidazolates containing iron ions (Fe^{2+} or Fe^{3+}) are involved in complex mechanisms of reactions such as photo, electro, ultrasonic, or combination processes. The relatively high saturation magnetization values of ZIF-67-Fe_3O_4NPs make it susceptible to magnetic fields and easy to separate from aqueous solutions. The absence of significant hysteresis, remanence, and ZIF-67-Fe_3O_4NPs is crucial for the adsorption and removal of materials [21–23]. In this ecological-focused article aimed at eliminating harmful substances from the environment, we investigated the potential of zeolitic imidazolate-67 (ZIF-67) modified with Fe_3O_4 nanoparticles for the removal of propylparaben from aqueous solutions using the adsorption method. We employed response surface methodology (RSM) to evaluate its efficacy. While ZIF-67 modified with nanoparticles has been explored as an adsorbent in previous studies, there is a notable lack of comprehensive and thorough research on the removal of harmful substances from the fashion industry wastewater through the synthesis of chemically-modified MOFs adsorbents. To address this gap in the literature, we conducted a study focusing on ZIF-67 modified with Fe_3O_4NPs, which play significant roles in complex reaction mechanisms involving photo, electro, ultrasonic, or combination processes. The results showed a substantial improvement in the adsorption efficiency of harmful substances from the fashion industry and various dyes present in different water sources.

Our research focused on the development of an environmentally-friendly and effective solution for the removal of propylparaben from wastewater. In this study, we investigated the synthesis of a novel adsorbent called ZIF-67 modified by Fe_3O_4NPs as a viable alternative to excessive or harmful adsorbents. Fig. 1 illustrates the structured propylparaben and its removal process using the developed adsorbent. To achieve optimal adsorption efficiency, we utilized RSM and examined the impact of various parameters, including pH, time, propylparaben concentration, and adsorbent dosage, on the adsorption process. The results provide compelling evidence of the capability of ZIF-67-Fe_3O_4NPs in effectively eliminating propylparaben from aqueous solutions.

2. Experimental set-up

2.1. Chemical and instruments

The chemicals and reagents used in the analyses, such as propylparaben (99.1%), 2-methyl imidazole (99%), cobalt nitrate (99.1%), sodium acetate (99%), iron chloride(II) (99.0%), and iron chloride(III) (98.0%) were purchased from Merck HPLC grade (Company, Germany). The applied instruments were as follows: dyes concentrations were determined using Jasco UV-Vis spectrophotometer Model V-530 (Jasco Company, Japan). Infrared spectra on a (PerkinElmer Company, Germany). Scanning electron microscopy (SEM: KYKY-EM3200, Hitachi Company, China), is used to study the morphology of samples.

2.2. Synthesis of ZIF-67 modified by Fe_3O_4NPs

Synthesis ZIF-67 Modified by Fe_3O_4NPs were as follows: first, 0.86 g of $FeCl_2{\cdot}4H_2O$, 2.35 g $FeCl_3{\cdot}6H_2O$ (molar ratio of Fe^{2+}: Fe^{3+} = 1:2), and 40 mL of NH_4OH (25%) solution is mixed and placed under N_2 gas for 2 h at 90°C under stirrer condition [24]. They use an ultrasonic bath. This solution was added to the solution containing, 0.36 g of $Co(NO_3)_2{\cdot}6H_2O$, and 0.75 g of 2-methylimidazole, and 0.4 g of HCOO-Na in 60 mL of methanol for ZIF-67. The mixture was refluxed at 60°C for 24 h under N_2 gas. After cooling to room temperature, the mixture was centrifuged (3,000 rpm, 15 min, 15°C). The solids were left to soak in methanol for 3 d, and the solution was exchanged with fresh methanol every 24 h. The solids were centrifuged until the supernatant was colourless and dried at 80°C. The sorbent ZIF-67 modified by Fe_3O_4NPs with an equal weight ratio, the stirring, and the sediment suspension in the laboratory for 2 h produced, shown in Fig. 2 [22–24].

2.3. Application of adsorbent in different natural water systems

To evaluate the practical applicability of the prepared adsorbent for propylparaben treatment, various water samples including different natural water systems, hospital wastewater, and river water (containing Na^+, K^+, Ca^{+2}, Mg^{+2} ions) were subjected to sorption experiments using the determined maximum sorption method parameters. For the preparation of the humic acid stock solution, 0.15 g of humic acid was dissolved in 1 L of deionized (DI) water at an appropriate pH. The resulting mixture was then subjected to ultrasonication for 1 h. The supernatant was filtered using a 0.22 m PTFE syringe filter to remove any undissolved humic acid particles, and the concentration of

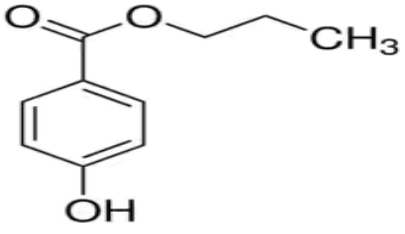

Fig. 1. Structures of propylparaben.

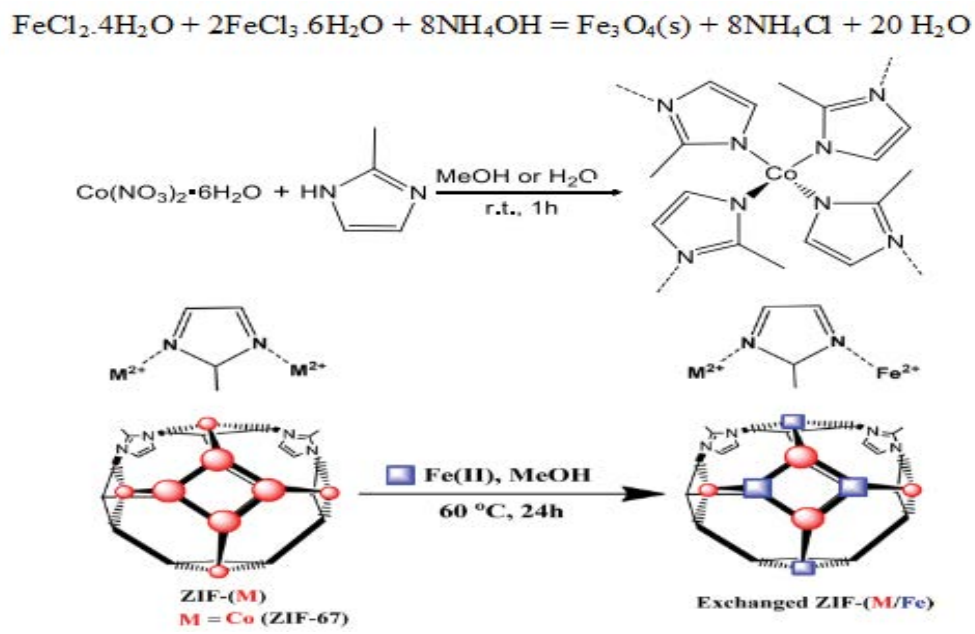

Fig. 2. Schematic representation of the synthesis of ZIF-67 modified by Fe_3O_4NPs.

humic acid in the filtered solution was determined. To prepare the propylparaben stock solution (100 mg·L^{-1}), 0.1 g of propylparaben was dissolved in 1 L of DI water. Adsorption experiments were conducted using 50 mL of 10 mg·L^{-1} propylparaben solutions obtained from hospital wastewater and river water, along with the optimal dosage and contact time, in order to compare the sorption performance against propylparaben-spiked deionized water.

2.4. Ultrasound assisted method

Generally, the sonochemical adsorption of propylparaben with ZIF-67 modified by Fe_3O_4NPs from aqueous solutions by adsorption method was studied using RSM, as follows: specified amounts of propylparaben solution (50 mL) at a known concentration (10.0 mg·L^{-1} for of propylparaben concentration, respectively) and pH 6.0 with a known amount of adsorbent (0.025 g) were loaded into the flask and maintained the desired sonication time (5 min) at the 25°C. It is worth mentioning that all utilized solutions were prepared per day with desired concentrations by diluting the stock solution with DW (double distilled water). The analysis of the dilute phase was done for determining propylparaben concentration with the help of a UV-Vis spectrophotometer at the wavelength of 390 nm. The computation of the removal percentage of propylparaben during a given period and the calculation of the amount of propylparaben adsorbed after reaching the equilibrium (q_e (mg·g^{-1})) was done using the ensuing equations:

$$R\% = \frac{C_0 - C_e}{C_0} \times 100 \quad (1)$$

$$q_i = \frac{V\left(C_0 - C_e\right)}{M} \times 100 \quad (2)$$

where C_0 is the propylparaben concentration at the time of adding the catalyst (mg·L^{-1}) and C_e is the remaining propylparaben concentration in the reaction time t (mg·L^{-1}). V (L) shows the solution [25,26].

2.5. Central composite design

To investigate the impact of various input variables on the response variables, we employed a central composite design (CCD) approach, as described in previous studies [10,31]. In this study, we considered propylparaben (X_1), pH (X_2), amount of adsorbent (X_3), and contact time (X_4) as the input variables, while the efficiency of propylparaben adsorption by ZIF-67 modified by Fe_3O_4NPs served as the response variable. The four independent variables were set at four different levels, and the corresponding propylparaben removal percentages (R%) were determined and recorded in Tables 1 and 2 [27,28].

3. Results and discussion

3.1. Characterization of sorbent

3.1.1. Brunauer–Emmett–Teller; analysis of ZIF-67 modified by Fe_3O_4NPs

Fig. 3 shows the related N_2 adsorption–desorption isotherm, which exhibits a type-IV isotherm with a noticeable hysteresis loop in the P/P_0 region of 0.3–0.95. The corresponding N_2 adsorption–desorption isotherm is in Fig. 3, where a type-IV isotherm is visible with a distinct hysteresis loop in the P/P_0 range of 0.2–0.97. Furthermore, for Fe_3O_4, the average pore diameter, pore volume, and specific surface area were observed to be 5.41 nm, 0.077 cm^3·g^{-1}, and 21.2 m^2·g^{-1}, respectively. Nevertheless, the values of the above parameters for ZIF-67-Fe_3O_4NPs were detected to be 3.17 nm, 0.612 cm^3·g^{-1}, and 942 m^2·g^{-1}, respectively [22,29].

Table 1
Experimental factors, levels, and matrix of central composite design

Factors	Levels			Star point α = 2.0	
	Low (–1)	Central (0)	High (+1)	–α	+α
(X_1) Propylparaben concentration (mg·L^{-1})	6.0	10.0	14.0	2.0	18.0
(X_2) pH	4.0	5.0	6.0	3.0	8.0
(X_3) Adsorbent dosage (g)	0.015	0.025	0.035	0.005	0.045
(X_4) Sonication time (min)	3.0	4.0	5.0	2.0	6.0

Table 2
Design and the response

Run	X_1	X_2	X_3	X_4	R% propylparaben
1	10	6	0.035	5	93.0
2	14	8	0.015	2	65.0
3	10	4	0.025	5	96.0
4	10	6	0.025	6	94.0
5	18	4	0.015	4	74.0
6	10	8	0.025	6	99.2
7	10	4	0.025	4	97.0
8	10	6	0.035	5	95.0
9	14	6	0.035	6	83.0
10	14	4	0.025	5	91.0
11	10	6	0.025	5	94.6
12	14	8	0.015	4	72.0
13	20	8	0.015	4	81.0
14	10	6	0.035	5	96.0
15	10	6	0.025	4	93.0
16	18	4	0.035	5	94.2
17	14	6	0.025	5	94.1
18	10	6	0.025	6	94.4
19	10	6	0.025	4	98.2
20	10	4	0.035	5	96.0
21	10	6	0.025	5	100.0
22	5	2	0.025	6	60.2
23	5	8	0.035	2	66.0
24	14	6	0.025	6	94.3
25	14	6	0.025	6	94.6
26	14	6	0.035	5	91.2
27	5	6	0.005	2	66.0
28	18	8	0.035	4	84.0
29	10	4	0.045	5	96.0
30	14	6	0.015	5	99.2

3.1.2. Fourier-transform infrared spectroscopy, X-ray diffraction, and scanning electron microscopy analysis

Fourier-transform infrared spectroscopy (FTIR), X-ray diffraction (XRD), and SEM measurements to characterize the adsorbent structural characterization. Fig. 4a, all FTIR spectra exhibit broadband covering the 3,300–3,500 cm^{-1} range, with an absorption band observed at 3,378 cm^{-1} for stretching vibrations of OH groups and C–H bonds,

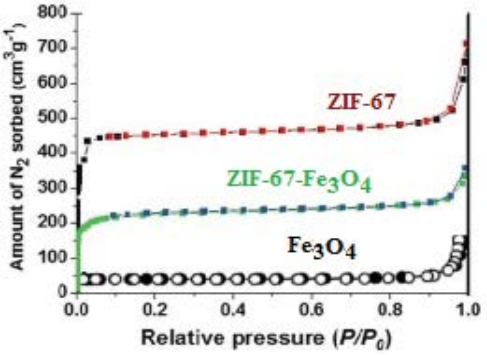

Fig. 3. Corresponding Barrett–Joyner–Halenda pore distribution curve of ZIF-67, Fe_3O_4NPs, ZIF-67-Fe_3O_4NPs.

respectively. The characteristic band at 1,590 cm^{-1} is consistent with the C=N stretching vibrations in ZIF-67. The FTIR spectra of ZIF-67-Fe_3O_4NPs showed distinct peaks of ZIF-67, indicating vibrations. The rise, at 1,055 and 1,392 cm^{-1} confirmed the presence of benzene rings. The peak was also, at 572 cm^{-1} for Fe–O–Fe bonds in the Fe_3O_4 nanoparticles [22,30]. The ZIF-67-Fe_3O_4NPs (b) XRD patterns to the standard Fe_3O_4 (a) XRD pattern. Two samples showed characteristic Fe_3O_4 peaks. An intense distinct diffraction peak can be for the traditional, patterns of Fe_3O_4 (JCPDS card #00-001-111) at 2θ = 63.06°, 57.23°, 53.73°, 43.34°, 35.75°, and 30.38°, respectively, corresponding to (440), (511), (422), (400), (311), and (220) planes. Furthermore, a diffraction peak at 2θ = 23.04 was observed in the ZIF-67-Fe_3O_4NPs (b) magnetic nanoparticles, corresponding to the dextrin coating of the Fe_3O_4 nanoparticles (Fig. 4b) [30,31]. A morphological study of the ZIF-67-Fe_3O_4NPs was carried out by SEM. The surface morphology of the ZIF-67-Fe_3O_4NPs is in Fig. 5. Clearly, the ZIF-67-Fe_3O_4NPs are formed of many ultrafine nanoparticles in the range of 36–55 nm [31,32].

3.2. Modeling process

Analysis of variance was performed to obtain information on the most important variables and their possible interactions (Table 3). Accordingly, to the model, very small p-values (<0.0001) for most terms indicated the high suitability and applicability of the model for prediction of propylparaben removal within a 95% confidence level. In an RSM model, the response variable (Y) is affected by several independent variables (X_1, X_2, X_3 and X_n). In RSM, the most complex model is the second-order or quadratic model, which

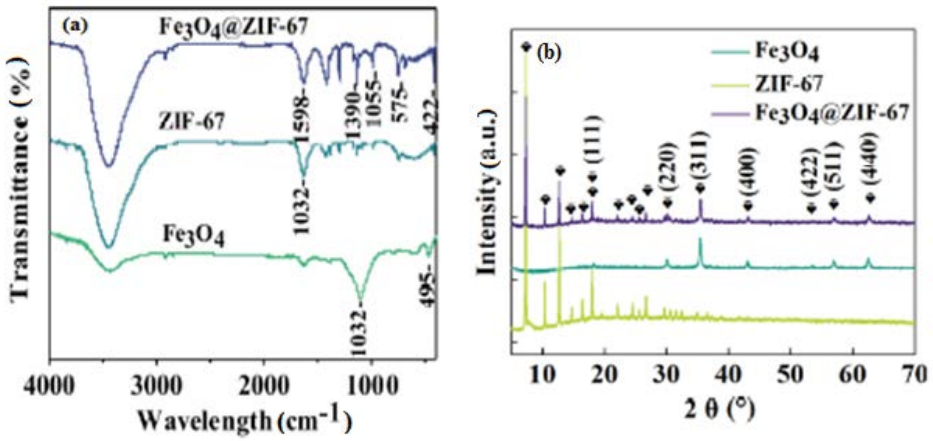

Fig. 4. (a) Fourier-transform infrared spectra of the prepared Fe_3O_4NPs, ZIF-67, ZIF-67-Fe_3O_4NPs. (b) Comparison of the X-ray diffraction pattern of Fe_3O_4NPs, ZIF-67, and ZIF-67-Fe_3O_4NPs.

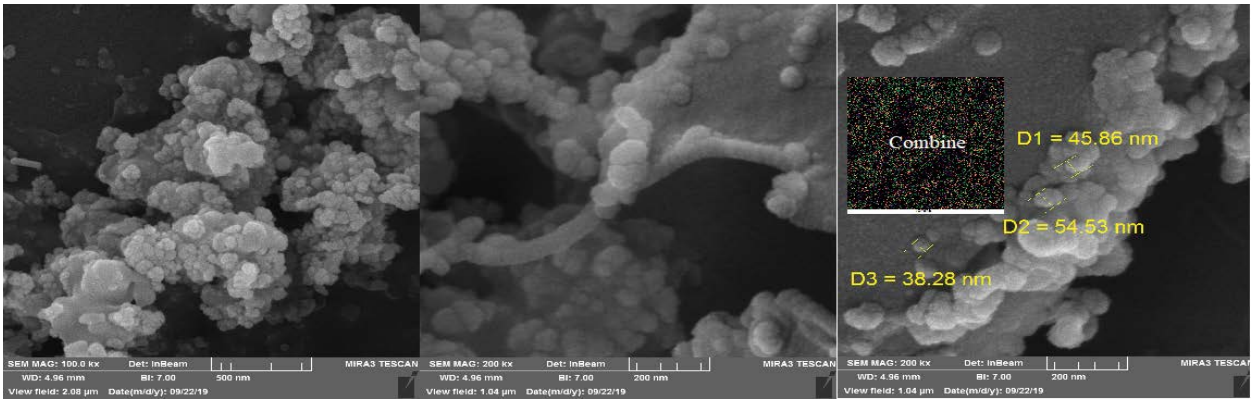

Fig. 5. Scanning electron microscopy image of the ZIF-67-Fe_3O_4NPs.

includes the relationship between response and independent variables (contains components such as first power, interactive impacts, polynomial function, and intercept point). The quadratic model is expressed by Eq. (3) [33,34].

$$\begin{aligned} R\%\ \text{of propylparaben} &= 96/281 - 10/121X_1 - 3/368X_2 \\ &+ 2/517X_3 + 4/281X_4 - 4/897X_1X_2 - 1/421X_1X_3 \\ &+ 3/572X_1X_4 + 0/9130X_2X_3 - 0/1770X_2X_4 \\ &- 0/43890X_3X_4 - 3/6988X_1^2 - 1/0951X_2^2 \\ &+ 0/4117X_3^2 \circledcirc 2/3611X_4^2 \end{aligned} \quad (3)$$

The value of the determination coefficient for predicting the function of propylparaben adsorption onto ZIF-67-Fe_3O_4NPs in Table 3.

3.3. RSM analysis

RSM to facilitate, the optimization and estimation of all significant interactions of variables and the relative significance of adsorption processes [34,35]. Fig. 6, clearly represents the level of each process parameter, optimal response values and experimental outcomes. The interaction of adsorbent mass with an initial concentration of propylparaben is represented in Fig. 6a. Increase in the adsorbent dosage led to a boost in the removal percentage on the grounds of the availability of more active adsorption sites and high specific surface area. In Fig. 6b and c the relevant interaction impact of sonication time on removal percentage is demonstrated. An increase was observed in the adsorption efficiency when time was increased under combined ultrasound/adsorbent process. Fig. 6d presents the interaction of pH with sonication time, respectively. The optimum conditions were as follows: pH of 6.0, ultrasound time of 5 min, adsorbent mass of 0.025 g, and initial propylparaben concentration equal to 10 mg·L^{-1} for removal propylparaben from aqueous media with the help of ZIF-67-Fe_3O_4NPs [36,37].

3.4. Optimization of CCD by DF for procedure

Desirability function (DF) creates a function for each individual response leading to final output of global function (*D*), maximum value of which supports the achievement of optimum value [34]. The desirability profiles indicate the predicted levels of variables, which produce the most desirable responses. The optimization of the process

Table 3
Analysis of variance for the full quadratic model

Source of variation	df	Propylparaben			
		Sum of square	Mean square	*F*-value	*p*-value
Model	14	4,353.5	312.12	756.66	<0.0001
X_1	1	1,799.8	1799.8	4,352.2	<0.0002
X_2	1	262.66	262.66	648.19	<0.0001
X_3	1	141.26	141.26	326.5	<0.0000
X_4	1	426.55	426.55	1,128.3	<0.0001
X_1X_2	1	363.6	363.6	927.2	<0.0002
X_1X_3	1	32.15	32.15	76.4	<0.0000
X_1X_4	1	213.4	213.4	467.4	<0.0001
X_2X_3	1	13.8	13.8	30.7	<0.0000
X_2X_4	1	0.468	0.468	1.1821	0.28266
X_3X_4	1	3.0891	3.0891	7.4732	0.0164
X_3X_5	1	225.22	225.22	564.16	<0.0001
X_1^2	1	34.015	34.015	82,133	<0.0001
X_2^2	1	4.3212	4.3212	10.56	0.00544
X_3^2	1	153.76	153.76	373.23	<0.0001
X_4^2	15	6.323	0.4312	752.12	<0.0002
Residual	9	5.1263	0.5633		
Lack of fit	6	1.0454	0.17822	3.312	0.078926
Pure error	29	4,361.6			
Cor. total					

(Fig. 7). The CCD design matrix results were obtained as maximum (100%) for propylparaben, respectively [34,37].

3.5. Adsorption isotherms

In this study, the relationship between the dye molecules adsorbed on the ZIF-67-Fe_3O_4NPs surface and the dye molecules remaining in the solution was investigated using widely used isotherm models such as Langmuir, Freundlich, and Temkin isotherms, is show in Table 4 [38,39]. The Langmuir and Freundlich, and Temkin models were estimated using Eqs. (4), (6), and (7), respectively. The shape of the isotherms (R_L) was calculated using Eq. (5) [40,41].

$$\frac{C_e}{q_e} = \frac{C_e}{q_{\max}} + \frac{1}{q_{\max}K_L} \tag{4}$$

$$R_L = \frac{1}{1 + K_L C_0} \tag{5}$$

$$\ln q_e = \ln k_f + \frac{1}{n}\ln C_e \tag{6}$$

$$q_e = B_T \ln C_e + B_T \ln A_T \tag{7}$$

where $q_{\max}$ is the adsorption capacity (mg·g^{-1}), K_L is the adsorption energy (L·g^{-1}), k_f and n are the Freundlich constants.

The value of R_L determines whether the adsorption process is irriversable (R_L = 0), desirable (0 < R_L < 1), linear (R_L = 1) or undesirable (R_L > 1) [24,40].

The value of n determines whether the adsorption process is lineer (n = 1), physical (n > 1), or chemical (n < 1) [41].

3.6. Adsorption kinetics

Adsorption kinetics were determined using the experimental results. Pseudo-first-order and second-order models were examined in the study [42,43]. In the study, Eq. (8) gives the linear form of the pseudo-first-order kinetic model:

$$\ln\left(q_e - q_t\right) = \ln q_e - k_1 t \tag{8}$$

where q_e and q_t are the adsorption capacity at the equilibrium state (mg·g^{-1}) and at any time (mg·g^{-1}), respectively. k_1 is the rate constant (min^{-1}), and calculated from the slope of the graph plotted against $\ln(q_e - q_t)$ vs. t [42].

Also, the pseudo-second-order kinetic model in Eq. (9):

$$\frac{t}{q_t} = \frac{t}{k_2 q_e^2} + \frac{t}{q_e} \tag{9}$$

where k_2 (g·mg^{-1}·min^{-1}) is the rate constant of the pseudo-second-order kinetic. Drawing the linear graph of t/q_t vs. t can provide the pseudo-second-order kinetic rate parameter [43].

Adsorption kinetics were determined using the experimental results of the adsorption of propylparaben onto ZIF-67-Fe_3O_4NPs in Table 5.

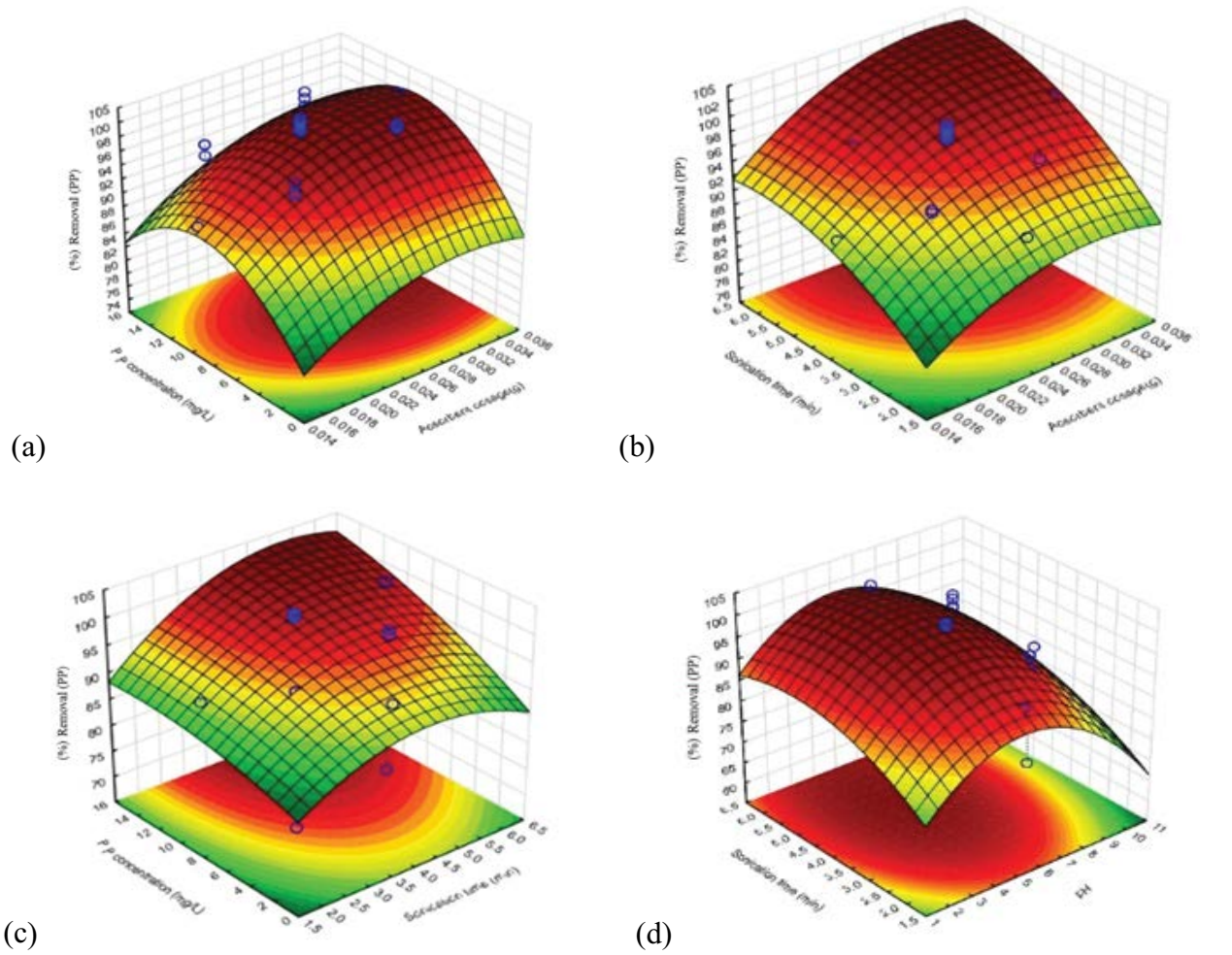

Fig. 6. Response surfaces for the propylparaben removal: (a) initial propylparaben concentration – adsorbent dosage, (b) sonication time – adsorbent dosage (c) initial propylparaben concentration – sonication time and (d) sonication time – pH.

3.7. Thermodynamics behaviour

Eqs. (10) and (11) were used to calculate the standart change of Gibbs free energy, enthalpy, and entropy in the adsorption process [44,45].

$$\Delta G^\circ = \Delta H^\circ - T\Delta S^\circ \tag{10}$$

$$\ln K_c = -\frac{\Delta G^\circ}{RT} = \frac{\Delta S^\circ}{R} - \frac{\Delta H^\circ}{RT} \tag{11}$$

The obtained values of ΔH°, ΔS°, and ΔG° in Table 6, and in general, the negative values of ΔG° at all working temperatures. So, $\Delta G^\circ < 0$ indicating that the studied adsorption process is spontaneous in the range of used temperature, $\Delta H^\circ < 0$ indicates that the study adsorption is exothermic [45,46].

3.8. Adsorption mechanism of propylparaben into ZIF-67-Fe_3O_4NPs

The adsorption mechanism of propylparaben onto the surface of ZIF-67-Fe_3O_4NPs can be deduced by analyzing the FTIR results. Based on the cationic nature of the dye and the negative surface charges of ZIF-67-Fe_3O_4NPs, favorable interactions are expected [23,46]. Fig. 8 illustrates the different potential interactions observed between propylparaben and the surface of ZIF-67-Fe_3O_4NPs.

3.9. Use of adsorbent for propylparaben removal from the water sample

In order to assess the effectiveness of the prepared sorbent in various matrices, spiked water samples from natural sources were treated with ZIF-67-Fe_3O_4NPs, and the results were compared to the sorption data obtained from spiked DI water (Fig. 9). Additionally, the influence of the common ion effect on propylparaben removal was evaluated by introducing a solution containing 50 mg·L^{-1} Na^+, K^+, Ca^{2+}, and Mg^{2+} ions spiked with 10 mg·L^{-1} of propylparaben. The results revealed propylparaben removal percentages of 90.2% in DI water, 77.9% in hospital wastewater, and 72.6% in river water. The relatively high removal percentage of propylparaben in natural water sources compared to DI water demonstrates the effective sorption ability of the sorbent in diverse sources. However, it is worth

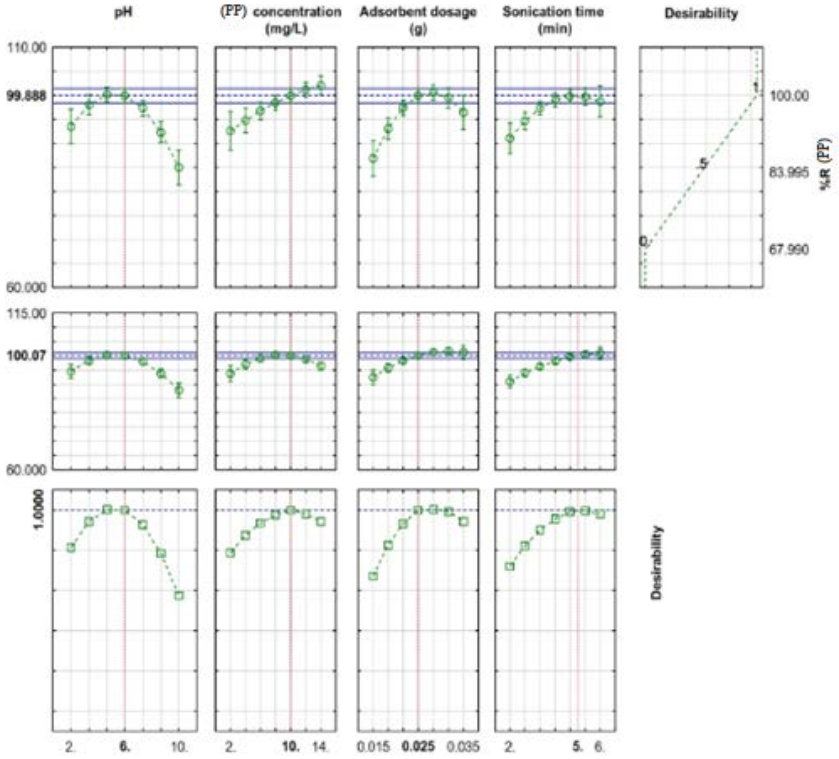

Fig. 7. Profiles for predicated values and desirability function for removal percentage of propylparaben line indicate current values after optimization.

Table 4
Adsorption isotherm models of propylparaben onto ZIF-67-Fe_3O_4NPs

Isotherm	Equation	Parameters	Value of parameters for propylparaben
Langmuir	$\frac{C_e}{q_e}=\frac{C_e}{q_{\max}}+\frac{1}{q_{\max}K_L}$	q_m (mg·g^{-1})	117.5
		K_L (L·mg^{-1})	0.564
		R^2	0.998
Freundlich	$\ln q_e=\ln k_f+\frac{1}{n}\ln C_e$	$1/n$	0.51
		k_f (mg)$^{1-n}$·L^n·g^{-1}	4.34
		R^2	0.973
Temkin	$q_e=B_1\ln K_T+B_1\ln C_e$	B_T (J·mol^{-1})	15.4
		K_T (L·mg^{-1})	6.825
		R^2	0.943

Conc. propylparaben = 10.0 mg·L^{-1}, pH = 6.0, dosage sorbent = 0.025 g, time = 5.0 min, T = 25°C.

noting that the river water sample exhibited lower propylparaben sorption compared to DI water, potentially due to the elevated levels of salts and other dissolved substances present in the river water [27,47].

3.10. Effect of humic acid for removal of propylparaben from wastewaters

The adsorption of propylparaben in hospital wastewater, and river water by ZIF-67-Fe_3O_4NPs adsorbent at different concentration of humic acid (mol·L^{-1}) is illustrated in Fig. 10. The concentrations 0.0–1.0 mol·L^{-1} of humic acid, were added to 50 mL of the tested individual beakers in optimal conditions 10 mg·L^{-1} initial concentration propylparaben, pH 6, 0.025 g adsorbent concentration, and 5 min contact time, respectively [43,47]. As the concentration of humic acid increases, the adsorption of propylparaben decreases. At pH less than 7, the propylparaben molecules were protonated, which neutralized a part of the humic acid molecules' electron cloud and it led to the reduction of humic acid and ZIF-67-Fe_3O_4NPs adsorption interactions. But no significant increase in the propylparaben adsorption capacity was observed under acidic conditions as a result of electrostatic repulsion force between humic acid and propylparaben molecules at pH 6. Due to competition for adsorption sites and the propylparaben molecules. The

ZIF-67-Fe_3O_4NPs pore blockage was caused by humic acid. This is because an increase in the ionic strength may cause the adsorbent particles to aggregate, resulting in a reduction in the adsorbent's functional adsorption sites, thus affecting its adsorption capabilities [8,48].

Table 5
Various kinetic constants and their correlation coefficients were calculated for the adsorption of propylparaben onto ZIF-67-Fe_3O_4NPs

Models	Parameters	Value of parameters for propylparaben
Pseudo-first-order kinetic	k_1 (min^{-1})	0.974
	$q_{e(calc)}$ ($mg·g^{-1}$)	17.66
	R^2	0.9212
Pseudo-second-order kinetic	k_2 (min^{-1})	0.147
	$q_{e(calc)}$ ($mg·g^{-1}$)	56.27
	R^2	0.9989

Conc. propylparaben = 10.0 $mg·L^{-1}$, pH = 6.0, dosage sorbent = 0.025 g, time = 5.0 min, T = 25°C.

3.11. Recyclability of the adsorbent

As can be seen from Fig. 11, the propylparaben removal efficiency decreased slightly with an increase in cycle number. After four cycles, the efficiency reduced from 99.19% to 71.67%. The result proved the stability of the ZIF-67-Fe_3O_4NPs for the degradation of propylparaben as the adsorption process. In addition, the decrease in the degradation

Table 6
Thermodynamic parameters for the adsorption of propylparaben onto ZIF-67-Fe_3O_4NPs

Parabens ($mg·L^{-1}$)	T (°K)	Value of $\Delta G°$ ($kJ·mol^{-1}$)	Value of $\Delta H°$ ($kJ·mol^{-1}$)	Value of $\Delta S°$ ($kJ·mol^{-1}·K^{-1}$)
Propylparaben (10 $mg·L^{-1}$)	298	–24.2	–33.3	–56.8
	308	–36.8		
	318	–50.9		
	328	–63.6		
	338	–78.6		

Conc. propylparaben = 10.0 $mg·L^{-1}$, pH = 6.0, dosage sorbent = 0.025 g, time = 5.0 min, T = 25°C.

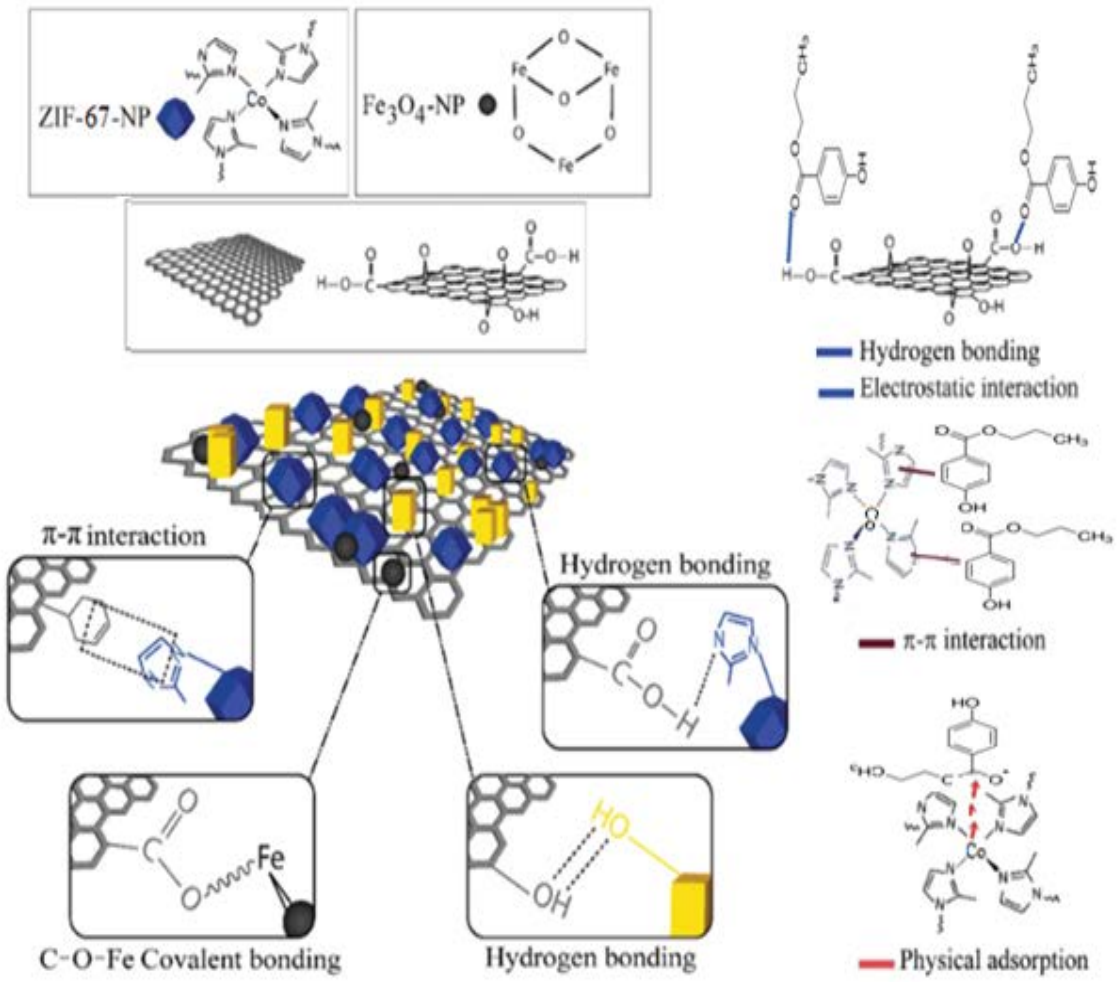

Fig. 8. Schematic presentation of the propylparaben adsorption mechanism onto surface ZIF-67-Fe_3O_4NPs.

Table 7
Comparison of results for this work with other reports

Paraben	Adsorbent	Dosage sorbent (g)	Adsorption capacity (mg·g^{-1})	References
Propylparaben	TiO_2 NPs-AC	0.025	120.0	[2]
Propylparaben	IL-MNP-βCD-TDI	0.02	18.48	[3]
Propylparaben	ALLC AgNPs	0.05	8.5	[6]
Propylparaben	ß-cyclodextrin (ß-CD) toluene-2,6-diisocyanate	0.1	0.1854 and 0.2551	[39]
Propylparaben	MWTACC	0.1	90.0	[44]
Propylparaben	*Origanum majorana*-capped AgNPs	0.05	93.0	[45]
Propylparaben	ZIF-67-Fe_3O_4NPs	0.025	117.5	Present study

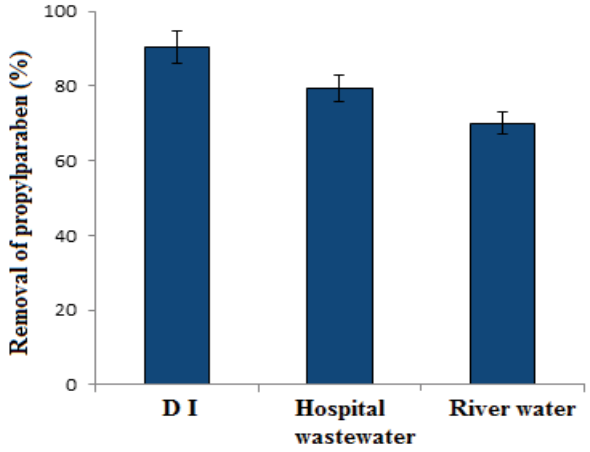

Fig. 9. Propylparaben removal from the deionized water, hospital wastewater, and river water (Na^+, K^+, Ca^{2+}, Mg^{2+} ions containing) water (n = 3). [Conc. propylparaben = 10.0 mg·L^{-1}, pH = 6.0, dosage sorbent = 0.025 g, time = 5.0 min, T = 25°C].

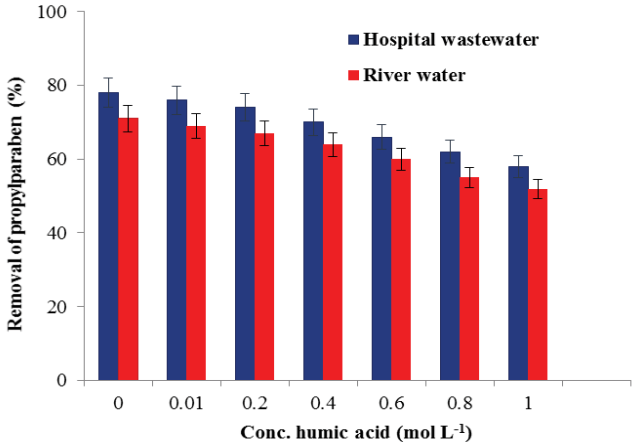

Fig. 10. Effect of humic acid on removing the propylparaben onto ZIF-67-Fe_3O_4NPs from the hospital wastewater, and river water. [Conc. propylparaben = 10.0 mg·L^{-1}, pH = 6.0, dosage sorbent = 0.025 g, time = 5.0 min, T = 25°C].

efficiency of propylparaben could by the adsorption of intermediates on the surface of ZIF-67-Fe_3O_4NPs [27,49].

3.12. Comparison of various adsorbent

A comparative of the maximum sorption capacity, q_{max} of ZIF-67-Fe_3O_4NPs with those of some other sorbents for adsorption propylparaben reported in literature is given in Table 7. Differences in q_{max} are due to the nature and properties of each sorbent such as surface area and the main functional groups in the structure of the sorbent. A comparison with other adsorbents indicated a high metal ion sorption capacity of ZIF-67-Fe_3O_4NPs.

4. Conclusion

The applicability of zeolitic imidazolate-67 modified by Fe_3O_4 nanoparticles was studied for removal of propylparaben from aqueous solutions by adsorption method was studied in a using RSM. The optimal values determined for propylparaben concentration, adsorbent mass, pH, and contact time were found to be 10 mg·L^{-1}, 0.025 g, 6.0 and 5.0 min, respectively. The experimental data were analyzed to determine the adsorption equilibrium and kinetics. The Langmuir isotherm and pseudo-second-order kinetics

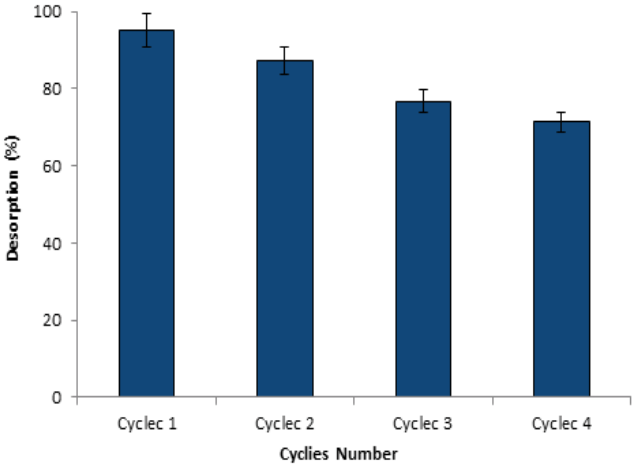

Fig. 11. Desorption of propylparaben from ZIF-67-Fe_3O_4NPs. [Conc. propylparaben = 10.0 mg·L^{-1}, pH = 6.0, dosage sorbent = 0.025 g, time = 5.0 min, T = 25°C].

were found to best fit the data, with a maximum adsorption capacity of 117.5 mg·g^{-1}. Thermodynamic parameters (ΔG°: –24.2 kJ·mol^{-1}, ΔH°: –33.3 kJ·mol^{-1}, ΔS°: –56.8 kJ·mol^{-1}·K^{-1}) further confirmed the feasibility, spontaneity, and

exothermic nature of propylparaben adsorption. The comparative adsorption removal of propylparaben from DI water, spiked natural water samples, and synthetic Na^+, K^+, Ca^{2+}, and Mg^{2+} solutions demonstrated the promising treatment capabilities of ZIF-67-Fe_3O_4NPs. Overall, considering its low cost, easy availability, and high removal efficiency, ZIF-67-Fe_3O_4NPs can be considered as a suitable adsorbent for the removal of propylparaben from aqueous solutions.

Acknowledgment

The authors would like to acknowledge and thank the partial support of the Islamic Azad University, Branch of Ayatollah Amoli, Iran in this work.

References

[1] B.P. Parihar, M. Chakraborty, S. Gupta, Application of pseudo-emulsion hollow fiber strip dispersion system for the removal of propylparaben from the aqueous solutions, Desal. Water Treat., 73 (2017) 301–307.
[2] M. Pargari, F. Marahel, B. Mombini Godajdar, Ultrasonic assisted adsorption of propyl paraben on uultrasonically synthesized TiO_2 nanoparticles loaded on activated carbon: optimization, kinetic and equilibrium studies, Desal. Water Treat., 212 (2021) 164–172.
[3] J. An, Ch. Xia, J. He, H. Feng, Oxidation of propyl paraben by ferrate(VI): kinetics, products, and toxicity assessment, J. Environ. Sci. Health., Part A, 53 (2018) 873–882.
[3] M. Md Yusoff, N. Yahaya, N. Md Saleh, M. Raoov, A study on the removal of propyl, butyl, and benzyl parabens *via* newly synthesised ionic liquid loaded magnetically confined polymeric mesoporous adsorbent, RSC Adv., 8 (2018) 25617–25635.
[4] F. Marahel, B. Mombeni Goodajdar, N. Basri, L. Niknam, A.A. Ghazali, Applying neural network model for adsorption methyl paraben (MP) dye using *Ricinus communis*-capeed Fe_3O_4NPs synthesized from aqueous solution, Iran. J. Chem. Chem. Eng., 41 (2022) 2358–2377.
[5] S. Habbal, B. Haddou, J. Cansellier, Easy removal of methylparaben and propylparaben from aqueous solution using nonionic micellar system, Tenside, Surfactants, Deterg., 56 (2019) 112–118.
[6] F. Maghami, M. Abrishamkar, B. Mombeni Goodajdar, M. Hossieni, Simultaneous adsorption of methylparaben and propylparaben dyes from aqueous solution using synthesized *Albizia lebbeck* leaves-capped silver nanoparticles, Desal. Water Treat., 223 (2021) 388–392.
[7] M.H. Bueno, N. Boluda-Botella, D.P. Rico, Removal of emerging pollutants in water treatment plants: adsorption of methyl and propylparaben onto powdered activated carbon, Adsorption, 25 (2019) 983–999.
[8] Z. Frontistis, Sonoelectrochemical degradation of propyl paraben: an examination of the synergy in different water matrices, Int. J. Environ. Res. Public Health, 17 (2020) 2621, doi: 10.3390/ijerph17082621.
[9] H.W. Chen, C.S. Chiou, Y.P. Wu, C.H. Chang, Y.H. Lai, Magnetic nanoadsorbents derived from magnetite and graphene oxide for simultaneous adsorption of nickel ion, methylparaben, and Reactive Black 5, Desal. Water Treat., 224 (2021) 168–177.
[10] F. Maghami, M. Abrishamkar, B. Mombini Godajdar, M. Hossieni, Green fabrication of *Albizia lebbeck* leaves-capped silver nanoparticles for removal of butylparaben, J. Appl. Chem. Res., 16 (2022) 45–64.
[11] H. Rashidi Nodeh, H. Sereshti, S. Ataolahi, A. Toloutehrani, A. Talesh Ramezani, Activated carbon derived from pistachio hull biomass for the effective removal of parabens from aqueous solutions: isotherms, kinetics, and free energy studies, Desal. Water Treat., 201 (2020) 155–164.
[12] D.Z. Husein, Facile one-pot synthesis of porous N-doped graphene based NiO composite for parabens removal from wastewater and its reusability, Desal. Water Treat., 166 (2021) 211–221.
[13] L. Rachid, B. Benamar, M. Farida, Removal of methyl orange from aqueous solution using zeolitic imidazolate framework-11: adsorption isotherms, kinetics and error analysis, Iran. J. Chem. Chem. Eng., 41 (2022) 1985–1999.
[14] M.A. Nazir, T. Najam, K. Zarin, Kh. Shahzad, M.S. Javed, M. Jamshaid, M.A. Bashir, S. Sh. Ahmad Shah, A. Ur Rehman, Enhanced adsorption removal of methyl orange from water by porous bimetallic Ni/Co MOF composite: a systematic study of adsorption kinetics, Int. J. Environ. Anal. Chem., 101 (2021) 1–20, doi: 10.1080/03067319.2021.1931855.
[15] Y. Si, W. Wang, E.M. El-Sayed, D. Yuan, Use of breakthrough experiment to evaluate the performance of hydrogen isotope separation for metal-organic frameworks M-MOF-74 (M = Co, Ni, Mg, Zn), Sci. China Chem., 63 (2020) 881–896.
[16] H. Wan, J. Wang, X. Sheng, J. Yan, W. Zhang, Y. Xu, Removal of polystyrene microplastics from aqueous solution using the metal-organic framework material of ZIF-67, Toxics, 10 (2022) 70–82.
[17] F. Xiao, J. Cheng, X. Fan, C. Yang, Y. Hu, Adsorptive removal of the hazardous anionic dye Congo red and mechanistic study of ZIF-8, Desal. Water Treat., 101 (2018) 291–300.
[18] J. Zhang, X. Yang, Sh. Cheng, D. Zou, F. Cheng, Preparation of core-shell TiO_2@ZIF-67 and its effective adsorption of methyl orange from water, Desal. Water Treat., 261 (2022) 266–277.
[19] A. Hajializadeh, M. Ansari, M. Foroughi, S. Jahani, M. Kazemipour, Zeolite imidazolate framework nanocrystals electrodeposited on stainless steel fiber for determination of polycyclic aromatic hydrocarbons, Iran. J. Chem. Chem. Eng., 41 (2022) 368–379.
[20] M.G. El-Desouky, A.A. El-Bindary, Magnetic metal-organic framework (Fe_3O_4@ZIF-8) nanocomposites for adsorption of anionic dyes from wastewater, Inorg. Nano-Metal Chem., 51 (2021) 1–17, doi: 10.1080/24701556.2021.2007131.
[21] Z. Wu, Y. Wang, Z. Xiong, Z. Ao, S. Pu, G. Yao, B. Lai, Core-shell magnetic Fe_3O_4@Zn/Co-ZIFs to activate peroxymonosulfate for highly efficient degradation of carbamazepine, Appl. Catal., B, 277 (2020) 119136, doi: 10.1016/j.apcatb.2020.119136.
[22] Z. Feng, J. Zhu, S. Zhuo, J. Chen, W. Huang, H. Cheng, L. Li, T. Tang, H. Feng, Magnetic/zeolitic imidazolate framework-67 nanocomposite for magnetic solid-phase extraction of five flavonoid components from Chinese herb *Dicranopteris pedata*, Molecules, 28 (2023) 702–714.
[23] P. Arabkhani, H. Javadian, A. Asfaram, M. Ateia, Decorating graphene oxide with zeolitic imidazolate framework (ZIF8) and pseudo-boehmite offers ultra-high adsorption capacity of diclofenac in hospital effluents, Chemosphere, 271 (2021) 129610, doi: 10.1016/j.chemosphere.2021.129610.
[24] L.E. Mphuthi, E. Erasmus, E.H.G. Langner, Metal exchange of ZIF-8 and ZIF-67 nanoparticles with Fe(II) for enhanced photocatalytic performance, ACS Omega, 6 (2021) 31632–31645.
[25] F. Mohammadi, A. Esrafili, H.R. Sobhi, M. Behbahani, M. Kermani, E. Asgari, Z. Rostami Fasih, Evaluation of adsorption and removal of methyl paraben from aqueous solutions using amino-functionalized magnetic nanoparticles as an efficient adsorbent: optimization and modeling by response surface methodology (RSM), Desal. Water Treat., 103 (2018) 248–260.
[26] F. Marahel, B. Mombeni Goodajdar, L. Niknam, M. Faridnia, E. Pournamdari, S. Mohammad Doost, Ultrasonic assisted adsorption of methylene blue dye and neural network model for adsorption of methylene blue dye by synthesized Mn-doped PbS nanoparticles, Int. J. Environ. Anal. Chem., 101 (2021) 1–22, doi: 10.1080/03067319.2021.1901895.
[27] Sh. Einolghozati, E. Pournamdari, N. Choobkar, F. Marahel, Response surface methodology for removal of methyl violet dye using *Albizia stem bark lebbeck* modified by $Fe_2(MoO_4)_3$ nanocomposite from aqueous solutions and assessment relative error by neural network model, Desal. Water Treat., 278 (2022) 195–208.
[28] M. Kiani, S. Bagheri, N. Karachi, E. Alipanahpour Dil, Adsorption of purpurin dye from industrial wastewater using

Mn-doped Fe_2O_4 nanoparticles loaded on activated carbon, Desal. Water Treat., 152 (2019) 366–378.
[29] A. Khan, M. Ali, A. Ilyas, P. Naik, I.F. Vankelecom, M.A. Gilani, M.R. Bilad, Z. Sajjad, A.L. Khan, ZIF-67 filled PDMS mixed matrix membranes for recovery of ethanol via pervaporation, Sep. Purif. Technol., 206 (2018) 50–64.
[30] Z. Zhao, G. Zhang, Y. Zhang, M. Dou, Y. Li, Fe_3O_4 accelerates tetracycline degradation during anaerobic digestion: synergistic role of adsorption and microbial metabolism, Water Res., 185 (2020) 116225, doi: 10.1016/j.watres.2020.116225.
[31] Y. Li, Z. Jin, T. Zhao, Performance of ZIF-67 – derived fold polyhedrons for enhanced photocatalytic hydrogen evolution, Chem. Eng. J., 382 (2020) 123051, doi: 10.1016/j.cej.2019.123051.
[32] X.D. Du, C.C. Wang, J.D. Liu, X.D. Zhao, J. Zhong, Y.X. Li, J. Li, P. Wang, Extensive and selective adsorption of ZIF-67 towards organic dyes: performance and mechanism, J. Colloid Interface Sci., 506 (2017) 437–447.
[33] M. El-Khomri, N. El-Messaoudi, A. Dbik, S. Bentahar, Y. Fernine, A. Lacherai, A. Jada, Optimization based on response surface methodology of anionic dye desorption from two agricultural solid wastes, Chem. Afr., 73 (2022) 1083–1095.
[34] S.A. Mosavi, A. Ghadi, P. Gharbani, A. Mehrizad, Optimization, kinetics and thermodynamics studies for photocatalytic degradation of methylene blue using cadmium selenide nanoparticles, J. Mater. Chem. Phys., 267 (2021) 124696, doi: 10.1038/s41545-022-00178-x.
[35] M. Kiani, S. Bagheri, A. Khalaji, N. Karachi, Ultrasonic supported deletion of Rhodamine B on ultrasonically synthesized zinc hydroxide nanoparticles on activated carbon concocted from wood of cherry tree: experimental design methodology and artificial neural network, Desal. Water Treat., 226 (2021) 147–156.
[36] A. Alipour Hajiagha, M. Zaeimdar, S.A. Jozi, N. Sajadi, A. Ghadi, Evaluation of efficiency and optimization of photo-Fenton process parameters in beet sugar wastewater treatment using response surface methodology (RSM), J. Environ. Sci. Technol., 24 (2022) 99–114.
[37] A. Rafiee, Sh. Ghanavati Nasab, A. Teimouri, Synthesis and characterization of pistachio shell/nanodiopside nanocomposite and its application for removal of crystal violet dye from aqueous solutions using central composite design, Int. J. Environ. Anal. Chem., 99 (2019) 1–26.
[38] S. Bagheri, H. Aghaei, M. Ghaedi, A. Asfaram, M. Monajemi, A.A. Bazrafshan, Synthesis of nanocomposites of iron oxide/gold (Fe_3O_4/Au) loaded on activated carbon and their application in water treatment by using sonochemistry: optimization study, Ultrason. Sonochem., 41 (2018) 279–287.
[39] Y.P. Chin, S. Mohamad, M.R. Bin Abas, Removal of parabens from aqueous solution using ß-cyclodextrin cross-linked polymer, Int. J. Mol. Sci., 11 (2010) 3459–3471.
[40] H.S. Ghazimokri, H. Aghaie, M. Monajjemi, M.R. Gholami, Removal of methylene blue dye from aqueous solutions using carboxymethyl-β-cyclodextrin-Fe_3O_4 nanocomposite: thermodynamics and kinetics of adsorption process, Russ. J. Phys. Chem. A, 96 (2022) 371–384.
[41] A.H. Jawad, A.S. Abdulhameed, L.D. Wilson, M.A.K.M. Hanafiah, W.I. Nawawi, Z.A. AL-Othman, M.R. Khan, Fabrication of Schiff's base chitosan-glutaraldehyde/activated charcoal composite for cationic dye removal: optimization using response surface methodology, J. Polym. Environ., 29 (2021) 2855–2868.
[42] M. Hubbe, S. Azizian, S. Douven, Implications of apparent pseudo-second-order adsorption kinetics onto cellulosic materials: a review, BioResources, 14 (2019) 7582–7626.
[43] Sh. Davoudi, Adsorption of methylene blue (MB) dye using NiO-SiO_2NPs synthesized from aqueous solutions: optimization, kinetic and equilibrium studies, Iran. J. Chem. Chem. Eng., 41 (2022) 2343–2357.
[44] G. Pertunia Mashile, A.M. Azile Nqombolo, K. Mogolodi Dimpe, N. Philiswa, N. Nomngongo, Recyclable magnetic waste tyre activated carbon-chitosan composite as an effective adsorbent rapid and simultaneous removal of methylparaben and propylparaben from aqueous solution and wastewater, J. Water Process Eng., 33 (2020) 101011, doi: 10.1016/j.jwpe.2019.101011.
[45] N. Karachi, S. Motahari, S. Nazarian, Working for the betterment of simultaneous deletion of paraben dyes from industrial effluents on to *Origanum majorana*-capped silver nanoparticles, Desal. Water Treat., 228 (2021) 389–402.
[46] A.H. Jawad, A.S. Abdulhameed, M.S. Mastuli, Acid-factionalized biomass material for methylene blue dye removal: a comprehensive adsorption and mechanism study, J. Taibah Univ. Sci., 14 (2020) 305–313.
[47] S. Boutemedjet, O. Hamdaoui, S. Merouani, Ch. Petrier, Sonochemical degradation of endocrine disruptor propylparaben in pure water, natural water, and seawater, Desal. Water Treat., 57 (2016) 27816–27826.
[48] A.R. Solaimany Nazar, M.B. Kurade, M. Ali Khan, B.H. Jeon, Effect of humic acid on adsorption of methylparaben from aqueous solutions onto commercially available granular activated carbons, Sci. Iran. C, 29 (2022) 1364–1376.
[49] Sh. Bouroumand, F. Marahel, F. Khazali, Removal of yellow HE_4G dye from aqueous solutions using synthesized Mn-doped PbS (PbS:Mn) nanoparticles, Desal. Water Treat., 223 (2021) 388–392.